

ORIGINAL RESEARCH ARTICLE

Titanium-doped graphite-type silicon carbide biosensor for detecting and eliminating gaseous pollution: A green chemistry approach by molecular simulation study

Fatemeh Mollaamin^{1,2}

¹ Department of Food Engineering, Faculty of Engineering and Architecture, Kastamonu University, Kastamonu 37100, Turkey; smollaamin@gmail.com

² Department of Biology, Faculty of Science, Kastamonu University, Kastamonu 37100, Turkey

ABSTRACT

Regarding thermal strength, chemical stability and surface reactivity of silicon carbide (SiC), it is possible to allocate it as a suitable gas detector for commercial application. Therefore, this research was focused on the investigation of the chemo-resistivity properties of SiC nanosheet through doping with the transition metal. Thermochemical, electric and magnetic properties of titanium (Ti)-doped graphene-like monolayer silicon carbide (SiC) sheet have been studied by the first-principles methods based on the density functional theory (DFT) for scavenging of gas molecules of CO, CO₂, NO, NO₂. The results recommend that the adsorption of these gas molecules on Ti-embedded monolayer SiC sheet is more energetically desired than that on the pristine ones. Gas molecules of CO, CO₂, NO, NO₂ have been adsorbed on the Ti site of doped monolayer SiC through the formation of covalent bonds. The assumption of chemical adsorptions has been approved by the projected density of states (PDOS) and charge density difference plots. Charge density difference calculations also indicate that the electronic densities were mainly accumulated on the adsorbate of CO, CO₂, NO, NO₂ gas molecules. The results in this investigation can indicate the competence of transition metal doped silicon carbide nanosheet in sensor devices.

Keywords: SiC; CO; CO₂; NO; NO₂; GM@Ti-SiC_sh; gas sensor; DFT

ARTICLE INFO

Received: 27 June 2023
Accepted: 1 August 2023
Available online: 8 October 2023

COPYRIGHT

Copyright © 2023 by author(s).
Applied Chemical Engineering is published by
EnPress Publisher, LLC. This work is licensed
under the Creative Commons
Attribution-NonCommercial 4.0 International
License (CC BY-NC 4.0).
<https://creativecommons.org/licenses/by-nc/4.0/>

1. Introduction

The practical application of two-dimensional (2D) material like graphene might be confined with small band gap. Thus, new 2D materials with perfect mechanical, thermoelectric, optical and electronic properties are the clue to the recent scientific investigations^[1-4]. Graphene with two-dimensional (2D) layered physical structure and the unique electronic properties has simulated a broad range of research enthusiasm on 2D materials which can be applied for the electronic, optoelectronic, and spintronic devices^[5-9]. In transition metal (TM) decorated carbon nanostructure, the TM-carbon binding takes place through a charge-transfer mechanism and the TM remains in the cationic state. Therefore, the gas molecule can get absorbed on the cationic transition metal element giving some electronic charge^[10-14].

The monolayer silicon carbide (SiC) as a new graphene-like semiconductor is a direct band gap material, while silicon being in the same group with the carbon represents attributes entirely analogous to that of carbon and makes it possible to generate powerful applications

in optoelectronic and electronic instruments^[15–20]. As the polarizability of Si is more than C, so it is expected that, due to stronger Van der Waal's interaction, SiC/Si nanosurface can bind compounds more strongly compared to the pure carbon nanostructures. It is known that for optimum adsorption of gas molecules, the ideal form of binding between the host material (SiC nanosheet) and adsorbed gas molecules should be intermediate between physisorption and chemisorption energy^[21–26].

In addition, transition metal (TM) atoms are considered to be the source of magnetism; in the results of TM-doped monolayer SiC, it can be found that the system can be a magnetic semiconductor by Co, Cu, Fe, Mn, and Ni doping^[27]. The TM dopants can cause a total Hamiltonian perturbation, eventually leading to changes in electronic structures, which makes it a substantial application in magnetic electronic devices^[28–34].

Recently, researchers have investigated the scavenging of several volatile organic compounds (VOCs) including 1,3-butadiene, benzene, p-xylene, indole and toluene on monolayer silicon carbide using density functional theory. The thermodynamic properties for the adsorption of VOCs on the monolayer SiC was measured by the adsorption energy computation. VOCs were observed in a plane parallel to monolayer SiC through C atoms due to the Van der Waal interactions between the VOCs and the monolayer SiC^[35].

Another work tried to compare the detecting capability of carbides containing SiC, GeC, SnC, and PbC for NO₂ removal. Theoretical parameters consisting of density of states, atomic charge, and frontier molecular orbital analysis using DFT method was investigated to understand the electronic attributes. The results have exhibited that SiC and GeC nanosheets are better NO₂ detectors compared to the SnC and PbC nanosheets^[36].

Moreover, a study has been done on the sensitivity of graphene, boron nitride, silicon carbide for carbon monoxide (CO) adsorption was by theoretical methods. The calculated properties of electrostatic potential, band energy gap extracts from frontier orbitals, atomic charge distributions have indicated that GRA/SiC hetero-structure is a potent sensor towards CO adsorption^[37].

Furthermore, the sensing treatment of SiC sheet through some toxic gases adsorption has been carried out. Among those data, it has been demonstrated that SiC sheet possess the gas molecule sensitivity in the order SO₂ > H₂S > NO₂ > NH₃ > HF > CO₂ > CO > NO > PH₃^[38].

In this research, it has been investigated the magnetic and electronic structures of Ti-doped graphene-like SiC sheet through adsorption of CO, CO₂, NO, NO₂ gas molecules (GM@Ti–SiC_sh) by using first-principle calculations based on the density functional theory (DFT)^[39]. The calculation is realized by generalized gradient approximation (GGA) potential and Perdew-Burke-Ernzerhof (PBE) functional^[40,41]. Therefore, we shall present the theoretical estimates for the charge transfer and the energy of binding with the SiC surface for adsorption of molecules. Let us note that there also exist some model approaches to the problem of adsorption in addition to the popular and currently widely used first-principles calculations.

2. Theoretical conception, material and methods

For the SiC graphene-like sheet calculation the sheet has been modeled by alternatively arranged 15 C and 15 Si atoms. In a previous theoretical calculation it is reported that the most stable structure of planar SiC forms graphene-like structure with alternative SiC bond and the bonding in such structure is of sp² type (**Figure 1**)^[42]. In our calculation, we have considered similar structure and optimized without any symmetry constraint.

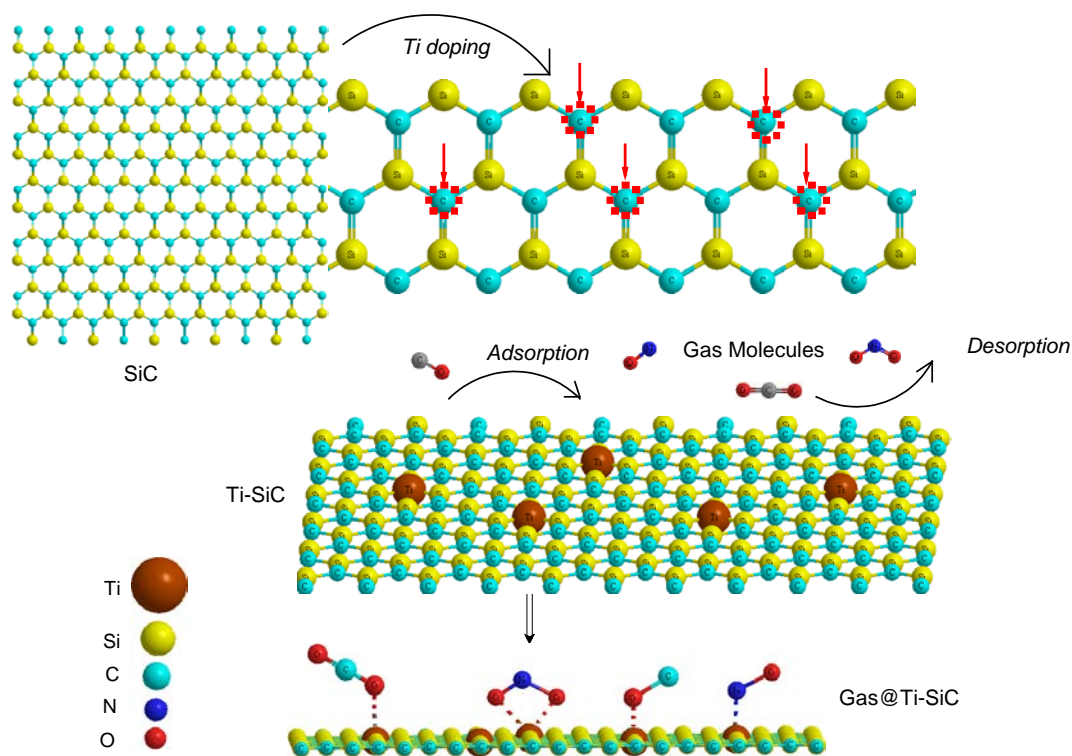


Figure 1. “Langmuir” adsorption of CO, CO₂, NO, and NO₂ onto Ti-doped SiC nanosheet.

The adsorbing of CO, CO₂, NO, NO₂ gas molecules on the surface of Ti–SiC_{sh} was defined by the theory “Langmuir” isotherm^[43,44], which indicates the chemisorption between gas molecules and Ti–SiC_{sh}. The adsorbates of CO, CO₂, NO, NO₂ gas molecules are maintained on surface of Ti–SiC_{sh} with “Langmuir” chemisorption (**Figure 1**).

In this research, the simulated calculations have been directed in the GaussView 6.06.16^[45] and calculated by Gaussian 16, Revision C.01^[46] using the density functional theory (DFT) method. The Perdew-Burke-Ernzerhof (PBE) functional with high-precision generalized gradient approximation (GGA) has been employed to achieve more authentic results^[47–52].

Besides, there are the limitations through using DFT method in estimating accurate vacancy formation energies in transition metals. The exceptional accord with the experiment received initially within DFT-LDA50 was later shown to result from a cancellation between two impacts. The structural relaxation, which was neglected, is now known to largely decrease the vacancy formation energy, especially in bcc metals^[53]. Second, DFT-LDA tends to underestimate the vacancy formation energy owing to the limitations of exchange-correlation functionals at surfaces. This discrepancy is even bigger within DFT-GGA, and it enhances with the number of valence electrons. It is accounted to be as large as 0.2 eV in LDA and 0.5 eV in GGA-PW1 for transition metals of Ni, Pd, and Pt, but it is smaller for transition metals of Ti, Zr, and Hf^[54].

The binding energy is calculated as: $E_b = (E_t - 15E_{Si} - 15E_C)/30$, where E_t is the total energy after optimization, E_{Si} and E_C are the correction factors for Si and C atoms, respectively.

From the charge density distribution of the SiC sheet, it is seen that a considerable amount of electronic charge is transferred from Si to C site. The presence of these point charges on the SiC sheet influences the gas adsorption property.

After organizing the structure and energetics of SiC sheet, we have tried to decorate the sheet by titanium atom. A full geometry optimization has been done and the data has explored that the most stable location of titanium is on the top of Si atom by pushing it down the surface.

Figure 1 has shown that the SiC sheet is distorted from planarity after adding the titanium in such a way that the doped titanium can bind with Si atom along with three neighboring carbon atoms, therefore developing the stability of the system. When the titanium atom is on the silicon atom, the Ti–Si bond distance is 2.56 Å while Ti–C bond distance is 1.98 Å. After doping of titanium on the silicon atom, the planarity of the system is perturbed because silicon atom goes toward the sp^3 hybridization. Although silicon and carbon atoms are iso-valent, the most stable state of carbon is sp^2 and silicon is sp^3 . Then, we have tailored the spin-polarized DFT calculation with our own N-layered Integrated Molecular Orbital and Molecular Mechanics (ONIOM) model^[55] accompanying the same force and energy convergence accuracy to the adsorption systems, with CAM-B3LYP functional and with 6-311+G (d,p)^[56] basis set for carbon, nitrogen, oxygen, silicon and LANL2DZ for titanium in the adsorption sites for the first layer (high level). Second layer (medium level) has been considered on some titanium atoms, carbon, and silicon atoms of SiC_sh, respectively, in the adsorption site due to semi-empirical methods. The third layer (low level) has been saved on the remained carbon and silicon atoms of SiC_sh with molecular mechanic force fields (**Figure 1**)^[55] as formula: $E_{\text{ONIOM}} = E_{1\text{st}} + E_{2\text{nd}} + E_{3\text{rd}}$.

It has been studied the interaction of CO, CO₂, NO, and NO₂ gas molecules with the Ti decorated SiC sheet. The optimized geometries of the GM@Ti decorated SiC sheet are shown in **Figure1**.

The charge transfer between adsorbates of CO, CO₂, NO, NO₂ and adsorbent of Ti–SiC_sh is calculated due to the Bader charge analysis^[57]. This method can measure charge accumulation from the charge of each atom in the complex model. Finally, the total adsorption charge transfer can be obtained as formula: $\Delta Q_i = Q_2 - Q_1$, where Q_2 and Q_1 remark the charge of CO, CO₂, NO, NO₂ before and after adoption, respectively. In fact, positive ΔQ_i indicates that electrons are transferred from gas molecules of CO, CO₂, NO, NO₂ to the surface of Ti–SiC_sh, and the adsorbent acts as an electron acceptor^[58,59].

The changes of charge density analysis in the adsorption process have illustrated that Ti–SiC_sh shows the Bader charge of $-1.307e$, before adsorption of CO, CO₂, NO, NO₂, and $-1.309e$, $-1.301e$, $-1.330e$, $-1.348e$ after adsorption of CO, CO₂, NO, NO₂, respectively. Therefore, the changes of charge density for Langmuir adsorption of CO, CO₂, NO, NO₂ on Ti–SiC_sh surface alternatively are $\Delta Q_{\text{CO}_2 \rightarrow \text{Ti-SiC}} = +0.006e > \Delta Q_{\text{CO} \rightarrow \text{Ti-SiC}} = +0.002e > \Delta Q_{\text{NO} \rightarrow \text{Ti-SiC}} = -0.023e > \Delta Q_{\text{NO}_2 \rightarrow \text{Ti-SiC}} = -0.041e$. The values of changes of charge density have shown a more important charge transfer for Ti–SiC_sh which acts as the electron acceptor while gas molecules act as the stronger electron donors through adsorption on the Ti–SiC_sh surface.

To determine the most sensitive structure of Ti–SiC_sh as the selective sensor for detecting gas molecules of CO, CO₂, NO, and NO₂, the binding energy of each system has been calculated. Therefore, we have found that the priority for selecting the surface binding of N-atom of NO, and O-atom of NO₂, CO, CO₂, in adsorption site can be impacted by the existence of close atoms in the Ti–SiC_sh surface. The simulated distribution functions of NO → Ti–SiC_sh, NO₂ → Ti–SiC_sh, CO → Ti–SiC_sh, and CO₂ → Ti–SiC_sh have illustrated that the created clusters lead to the bond lengths of N → Ti in NO → Ti–SiC_sh (2.07Å), O → Ti in NO₂ → Ti–SiC_sh (2.06Å), O → Ti in CO → Ti–SiC_sh (2.05Å) and O → Ti in CO₂ → Ti–SiC_sh (2.05Å) (**Figure 1**).

3. Results and discussions

These measurements in this article have been accomplished using spectroscopy analysis through some physical and chemical properties. In this verdict, titanium (Ti) metal-doped graphene-like monolayer silicon carbide (SiC) sheet has been investigated as the efficient surface because of their structural selectivity for adsorption of carbon monoxide (CO), carbon dioxide (CO₂), nitric oxide (NO), and nitrogen dioxide (NO₂).

3.1. Electronic properties

The electronic structures of CO, CO₂, NO and NO₂ adsorbed on the Ti-doped SiC nanosheet (GM@Ti-SiC_sh) have been analyzed to simplify subsequent discussion for interfacial electronic properties using CAM-B3LYP/LANL2DZ, 6-311+G (d,p) basis sets.

Figure 1 shows the projected density of state (PDOS) of the Ti decorated SiC sheet. The appearance of the energy states (*d*-orbital) of Ti within the gap of SiC sheet induces the reactivity of the system. It is clear from the figure that after doping with Ti atom and there is a significant contribution of Ti *d*-orbital in the unoccupied level. Based on the population analysis and DOS it can be concluded that Ti remains in the cationic state and it can accept more electrons from other atoms. Therefore, the graph of partial DOS (PDOS) has illustrated that the *p* states of the adsorption of N⁻ and O⁻ on the Ti-SiC_sh are dominant through the conduction band (**Figure 2**). A distinct metallic feature can be observed in SiC_sh because of the strong interaction between the *p* states of C, N, O, Si and the *d* state of Ti near the Fermi energy. Moreover, the existence of covalent features for these complexes has exhibited the identical energy amount and figure of the PDOS for the *p* orbitals of C, N, O, Si and *d* orbitals of Ti (**Figure 2a-d**).

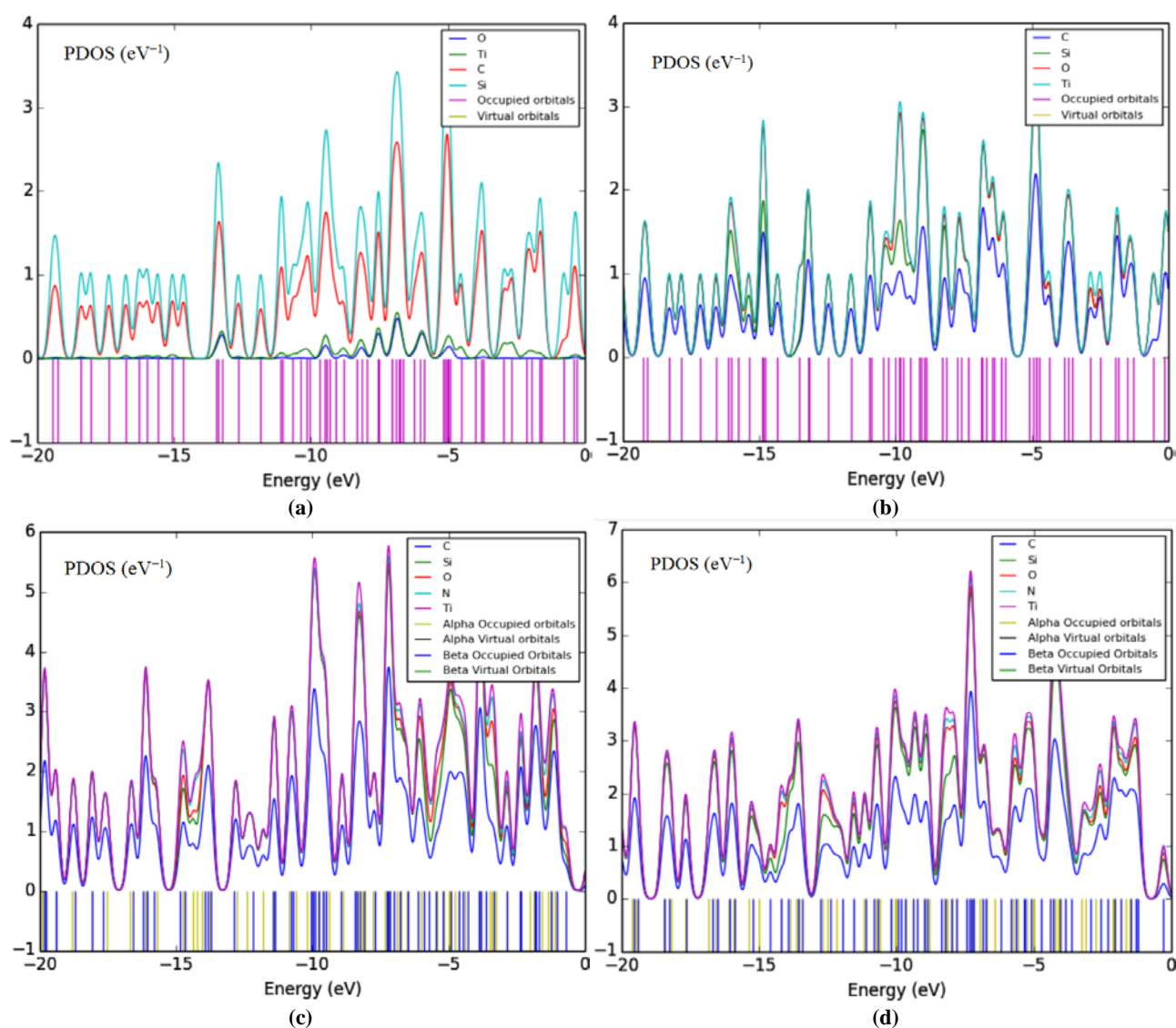


Figure 2. PDOS adsorption of (a) CO@Ti-SiC_sh; (b) CO₂@Ti-SiC; (c) NO@Ti-SiC; and (d) NO₂@Ti-SiC.

Figure 2a,b shows that the CO and CO₂ states, respectively, onto Ti–SiC_{sh} have more contribution at the middle of the conduction band between –5 eV to –10 eV, while contribution of carbon and silicon sates are expanded and close together, but titanium states have minor contributions.

Figure 2c,d shows that the NO and NO₂ states, respectively, onto Ti–SiC_{sh} have more contribution at the middle of the conduction band between –5 eV to –10 eV, while contribution of carbon and silicon sates are expanded and close together, but titanium states have major contributions.

The results also approved by the partial electron density (PDOS) which have showed a certain charge association between Ti–SiC_{sh} and gas molecules of CO, CO₂, NO and NO₂.

Therefore, the above results exhibit that the cluster dominant of non-metallic and metallic features and a certain degree of covalent features can illustrate the increasing of the semiconducting direct band gap of gas molecules of CO, CO₂, NO and NO₂ adsorbing on Ti–SiC_{sh}.

3.2. NQR “nuclear quadrupole resonance” analysis

NQR procedure has been done out for the complexes of gas molecules of CO, CO₂, NO and NO₂ adsorbing on Ti–SiC_{sh}. NQR is related to the multipole enlargement in cartesian harmonics as follows^[60,61]. There are two factors which should be gotten from nuclear quadrupole resonance experiments; the quadrupole coupling constant, χ , and asymmetry factor of the electric field gradient tensor η ^[62,63]. Since the electric field gradient at the situation of NO and NO₂ adsorbed on the Ti–SiC_{sh} surface as the gas detector is approved by the valence electrons distorted in the special connection with close nuclei of Ti-doped SiC nanosheet, the nuclear quadrupole resonance at which transitions occur is special for NO@Ti–SiC_{sh} and NO₂@Ti–SiC_{sh} (**Table 1**).

Furthermore, in **Table 1**, it has been drawn the electric potential of nuclear quadrupole resonance method versus Bader charge for elements of carbon, nitrogen, oxygen, silicon and titanium in the adsorption process of NO and NO₂ on the Ti-doped SiC nanosheet by CAM-B3LYP/EPR-III, 6-311+G (d,p), LANL2DZ theoretical level. It has been remarked the changes of electric potential for carbon, nitrogen, oxygen, silicon and titanium in the active site of Langmuir adsorption. In fact, it has been observed the effect of the binding between C, N and O atoms of gas molecules with titanium doping in the SiC nanosheet during adsorbing NO and NO₂ through resulted electric potential using NQR analysis (**Table 1**). It’s obvious that the capability of SiC nanosheet for detecting of NO and NO₂ is fluctuated by their selectivity and sensitivity which can represent the efficiency of these surfaces as the promising sensors (**Table 1**).

Table 1. The electric potential (Ep) and Bader charge (Q) for elements involving in the adsorption mechanism of NO and NO₂ adsorbed on the Ti-doped SiC nanosheet using CAM-B3LYP/EPR-III, 6-311+G (d,p) calculation extracted of NQR method.

NO@Ti–SiC _{sh}			NO ₂ @Ti–SiC _{sh}		
Atom	Q	Ep	Atom	Q	Ep
O1	–0.11602	–22.0984	N1	–0.19692	–18.1387
N2	–0.22516	–18.2494	O2	–0.16375	–21.8078
C3	–0.84948	–14.8598	O3	–0.10535	–21.9782
Si4	0.791873	–48.6641	C4	–0.83962	–14.8468
C5	–0.81214	–14.8302	Si5	0.795771	–48.6525
Si6	1.155139	–48.5961	C6	–0.82811	–14.8278
C7	–0.83718	–14.9081	Si7	1.209829	–48.5438
C8	–0.91859	–14.8321	C8	–0.82638	–14.8809
Si9	1.194218	–48.5956	C9	–0.89407	–14.817
Si10	1.19059	–48.5954	Si10	1.159963	–48.5914

Table 1. (Continued).

NO@Ti-SiC_sh			NO ₂ @Ti-SiC_sh		
Atom	Q	E _p	Atom	Q	E _p
C11	-0.85058	-14.8624	Si11	1.197638	-48.5827
C12	-1.1988	-14.785	C12	-0.84047	-14.8465
Si13	0.800878	-48.6357	C13	-1.20069	-14.7818
Si14	1.32384	-48.5129	Si14	0.821186	-48.6232
C15	-0.90157	-14.8175	Si15	1.347521	-48.4816
C16	-0.90257	-14.8232	C16	-0.84815	-14.6962
Ti17	0.305121	-90.4117	C17	-0.88875	-14.8371
Si18	1.173498	-48.5843	Ti18	0.445794	-90.3755
C19	-0.80896	-14.878	Si19	1.17213	-48.5887
C20	-1.22804	-14.7708	C20	-0.83124	-14.8991
Si21	0.904364	-48.5752	C21	-1.22568	-14.7855
Si22	1.30496	-48.503	Si22	0.844443	-48.6149
C23	-1.24856	-14.8287	Si23	1.30414	-48.5097
C24	-1.19829	-14.7793	C24	-1.24654	-14.8154
Si25	1.330167	-48.5044	C25	-1.19993	-14.785
Si26	0.796589	-48.6375	Si26	1.291316	-48.5139
C27	-0.82234	-14.8369	Si27	0.800832	-48.6358
C28	-0.86033	-14.7703	C28	-0.82404	-14.8373
Si29	0.917298	-48.5441	C29	-0.86755	-14.8003
Si30	0.890285	-48.5625	Si30	0.893514	-48.5776
C31	-1.23292	-14.7826	Si31	0.854561	-48.5954
Si32	0.932717	-48.5653	C32	-1.23148	-14.7995
-	-	-	Si33	0.920065	-48.579

3.3. Magnetism of gas adsorption onto Ti-Doped monolayer SiC

Isotropic (σ_{iso}) and anisotropy (σ_{aniso}) shielding tensors of nuclear magnetic resonance (NMR) spectroscopy for certain atoms in the active site of CO, CO₂, NO and NO₂ adsorbed on the Ti-doped SiC nanosheet (GM@Ti-SiC_sh) through the formation of the binding between gas molecules and solid surfaces have been calculated using Gaussian 16, Revision C.01 and reported in **Table 2**^[46].

Table 2. Data of gauge-independent atomic orbital (GIAO)/NMR shielding tensors for selected atoms of CO, CO₂, NO and NO₂ adsorbed on the Ti-doped SiC nanosheet (GM@Ti-SiC_sh) using CAM-B3LYP/EPR-III, 6-311+G (d,p) calculation.

CO@Ti-SiC_sh			CO ₂ @Ti-SiC_sh			NO@Ti-SiC_sh			NO ₂ @Ti-SiC_sh		
Atom	σ_{iso}	σ_{aniso}	Atom	σ_{iso}	σ_{aniso}	Atom	σ_{iso}	σ_{aniso}	Atom	σ_{iso}	σ_{aniso}
C1	11,111.4472	24,988.0432	C1	145.4006	210.9101	O1	2336.2195	2980.2105	N1	65.1036	342.5979
O2	2479.6300	5187.8214	O2	299.6111	162.9497	N2	805.0526	1027.1995	O2	235.4150	158.3215
C3	907.6908	2420.3768	C3	425.5927	1178.2736	C3	60.1550	315.5590	O3	141.4255	1217.9976
Si4	2088.0883	5367.7686	Si4	99.7387	972.5214	Si4	423.5479	333.0246	C4	76.0664	247.2353
C5	74.4146	412.2807	C5	81.6083	514.4560	C5	63.3853	473.6899	Si5	388.3425	406.7643
Si6	878.0865	1854.4291	Si6	538.7382	402.3132	Si6	547.1460	205.2232	C6	81.5389	511.2567
C7	2715.9557	11,547.4885	C7	1311.6230	2196.3916	C7	44.5324	166.3661	Si7	569.9207	198.6516
C8	1488.6353	3719.2313	C8	532.4831	967.7295	C8	15.1484	506.9911	C8	31.5175	182.2533
Si9	520.3949	558.6553	Si9	531.8902	308.3004	Si9	548.1179	180.5936	C9	152.4698	166.3381

Table 2. (Continued).

CO@Ti-SiC_sh			CO ₂ @Ti-SiC_sh			NO@Ti-SiC_sh			NO ₂ @Ti-SiC_sh		
Atom	σ_{iso}	σ_{aniso}	Atom	σ_{iso}	σ_{aniso}	Atom	σ_{iso}	σ_{aniso}	Atom	σ_{iso}	σ_{aniso}
Si10	427.4353	538.1887	Si10	487.2460	286.5483	Si10	498.9470	181.7101	Si10	503.5350	189.7524
C11	694.0893	4169.9333	C11	100.8839	899.6612	C11	125.0332	225.3520	Si11	493.1364	180.3917
C12	528.5808	995.4705	C12	184.0750	154.0651	C12	222.1382	60.0991	C12	95.9930	249.4879
Si13	109.4815	1142.8126	Si13	372.8765	679.4168	Si13	312.1764	666.1447	C13	250.0360	167.7335
Si14	812.7671	1834.8867	Si14	470.0050	470.0050	Si14	488.9875	112.7812	Si14	201.5410	943.1709
C15	390.8768	2337.0998	C15	279.4190	225.3213	C15	81.7264	242.3315	Si15	440.5262	230.2631
C16	324.1900	1766.0828	C16	267.3022	392.7469	C16	12.5167	393.1278	C16	110.0590	160.4944
Ti17	4441.5114	12,062.8971	Ti17	0.2898	2319.4610	Ti17	2193.9940	2915.8766	C17	152.9803	121.2933
Si18	684.7339	453.4367	Si18	470.7647	362.8494	Si18	534.7415	226.7653	Ti18	486.5292	524.9393
C19	3713.7019	13,466.0765	C19	986.2897	1699.6083	C19	43.8868	308.6632	Si19	489.9162	203.0216
C20	3310.0396	5480.1033	C20	405.8085	542.9896	C20	141.5596	145.6224	C20	22.7374	179.8416
Si21	2703.7518	8957.9647	Si21	159.6671	1012.0255	Si21	253.2383	205.2387	C21	30.6631	306.4868
Si22	976.7021	1668.0964	Si22	480.8095	208.0491	Si22	395.1189	187.6411	Si22	413.6272	1393.2065
C23	390.9605	743.8175	C23	235.0254	155.6737	C23	220.3842	94.5052	Si23	547.1171	299.1860
C24	25.5229	422.1970	C24	105.0097	268.4400	C24	198.8207	112.7170	C24	243.0867	158.9151
Si25	966.9951	1989.1605	Si25	460.0616	135.8942	Si25	519.6984	174.5462	C25	193.7582	127.3018
Si26	70.1612	70.1612	Si26	367.2007	441.4413	Si26	274.7445	749.6234	Si26	512.3460	205.8624
C27	44.7974	660.3342	C27	63.9877	576.2052	C27	119.1342	596.1158	Si27	330.7595	720.5845
C28	9184.2751	27,936.5520	C28	951.7545	1628.9741	C28	100.1434	587.8998	C28	129.3061	602.9246
Si29	11,614.9608	34,892.0907	Si29	667.8744	1743.8550	Si29	124.7423	430.1404	C29	248.4134	359.0231
Si30	11,034.4753	32,697.5319	Si30	850.2937	2044.8832	Si30	131.5901	359.0858	Si30	783.4974	1414.9085
C31	3090.8008	5299.2386	C31	476.3385	756.2754	C31	142.2919	81.5811	Si31	658.5249	1384.6970
Si32	1802.3087	6359.0112	Si32	98.2057	701.4854	Si32	314.3669	272.1731	C32	110.2182	121.6634
-	-	-	O33	235.2252	248.2998	-	-	-	Si33	558.9451	1001.1969

Isotropic chemical-shielding (σ_{iso}) & anisotropic chemical-shielding (σ_{aniso})[64]: $\sigma_{iso} = (\sigma_{33} + \sigma_{22} + \sigma_{11})/3$; $\sigma_{aniso} = \sigma_{33} - (\sigma_{22} + \sigma_{11})/2$.

The resulted graphs of NMR data in **Table 2** have shown approximately the identical chemical shielding behavior of isotropic and anisotropy factors of GM@Ti-SiC_sh with several sharp peaks related to carbon, nitrogen, oxygen, silicon and titanium of gas molecules (adsorbate) and TM-doped SiC nanosheet (adsorbent) in the active site situations. CO@Ti-SiC_sh with several sharp peaks related to the adsorption site for atoms including C1, C7, C11, C19, C28, Si4, Si21, Si29, Si30, Ti17; CO₂@Ti-SiC_sh with several sharp peaks for atoms of C7, C11, C19, C28, Si13, Si21, Si29, Si30, Ti17; NO@Ti-SiC_sh with several sharp peaks for atoms of O1, N2, Ti17 and several less sharp peaks for atoms of C5, C8, C28, Si13, Si26; and NO₂@Ti-SiC_sh with several sharp peaks for atoms of O3, Si14, Si22, Si27, Si30, Si31, and several less sharper peaks of N1, C6, Ti18, respectively, have been indicated.

Although, in the NMR spectroscopy, it has been observed the remarkable peaks around silicon and titanium atoms in the SiC nanosheets through the adsorption procedure of gas molecules, there are some fluctuations in the chemical shielding behaviors of isotropic and anisotropy attributes.

3.4. Vibrations of gas adsorption onto Ti-Doped monolayer SiC

In this part, the stability of complexes including gas adsorption on titanium (Ti) metal-doped graphene-like monolayer silicon carbide (SiC) sheet has been investigated through thermodynamic properties which define the reactions that CO, CO₂, NO, and NO₂ endure in the Ti-SiC_sh coordination sphere. Concerning adsorption process, the thermodynamic characters were evaluated for CO, CO₂, NO, and NO₂ on

the surface of Ti–SiC_{sh} as the gas detectors which can be applicable as the selective sensors for these gases (**Table 3**).

Table 3. The thermodynamic character of CO, CO₂, NO, and NO₂ adsorbed on the Ti–SiC_{sh} as the selective gas sensors.

Compound	$\Delta E^\circ \times 10^{-4}$ (kcal/mol)	$\Delta H^\circ \times 10^{-4}$ (kcal/mol)	$\Delta G^\circ \times 10^{-4}$ (kcal/mol)	S° (Cal/K mol)	Dipole moment (Debye)
CO	-6.9784	-6.9784	-6.9798	47.100	0.2373
CO ₂	-11.6121	-11.6121	-11.6136	51.378	0.0000
NO	-8.0017	-8.0016	-8.0031	48.968	0.2376
NO ₂	-12.6298	-12.6298	-12.6315	57.792	0.2323
SiC _{sh}	-304.3389	-304.3389	-304.3417	93.684	9.6011
Ti–SiC _{sh}	-339.1002	-339.1001	-339.1029	93.419	10.1407
CO@Ti–SiC _{sh}	-346.1065	-346.1064	-346.1093	97.616	10.3155
CO ₂ @Ti–SiC _{sh}	-350.7642	-350.7642	-350.7671	100.038	10.0483
NO@Ti–SiC _{sh}	-347.1429	-347.1428	-347.1458	100.033	16.4330
NO ₂ @Ti–SiC _{sh}	-351.8006	-351.8006	-351.8036	102.455	16.1658

Furthermore, the infrared (IR) spectrums for adsorption of CO, CO₂, NO, and NO₂ on the surfaces of Ti–SiC_{sh} have been reported in **Figure 3a–d**. The graph of **Figure 3a** has been observed in the frequency range between 500 cm⁻¹–2500 cm⁻¹ for the complex of CO@Ti–SiC_{sh} with a sharp peak around 545.09 cm⁻¹.

Figure 3b has shown the several strongest IR peaks of CO₂@Ti–SiC_{sh} approximately between 1000 cm⁻¹–3000 cm⁻¹ with a sharp peak of around 3048.47 cm⁻¹. **Figure 3c** has shown the several less stronger IR peaks of NO@Ti–SiC_{sh} approximately between 1500 cm⁻¹–2500 cm⁻¹ with a sharp peak of around 1730.07 cm⁻¹. **Figure 3d** has shown the several less stronger IR peaks of NO₂@Ti–SiC_{sh} approximately between 1500 cm⁻¹–2500 cm⁻¹ with a sharp peak of around 1823.63 cm⁻¹.

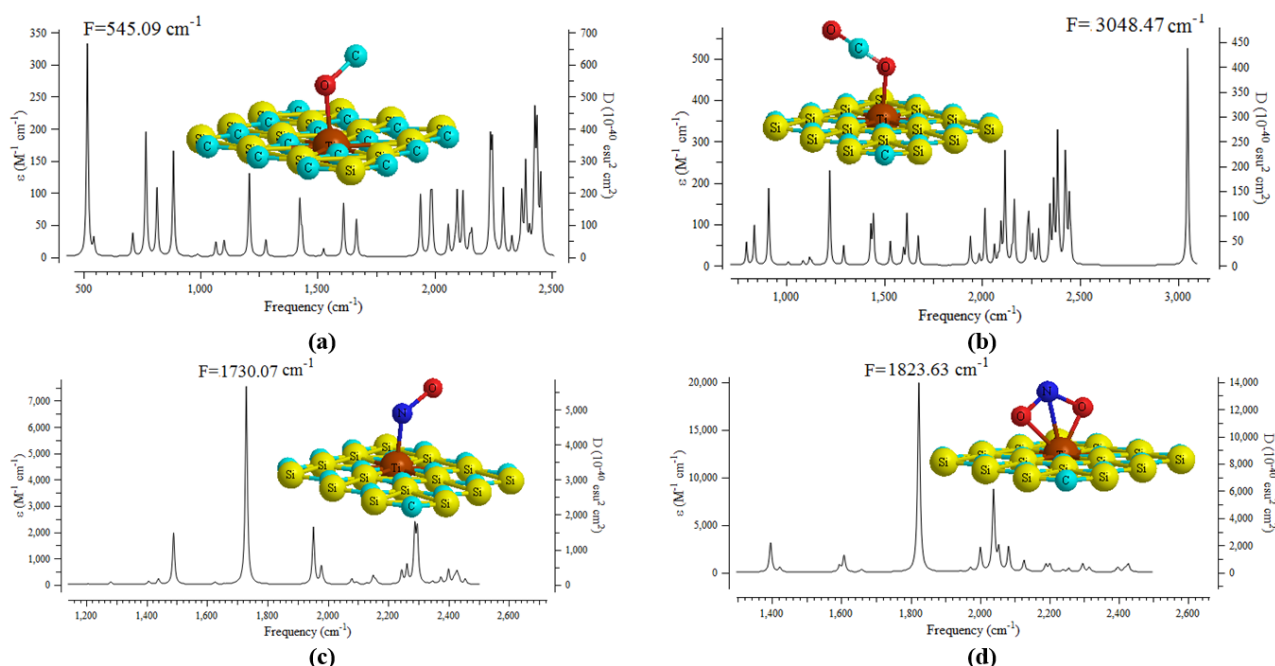


Figure 3. The frequency (cm⁻¹) changes through the “IR” spectrums for (a) CO@Ti–SiC_{sh}; (b) CO₂@Ti–SiC_{sh}; (c) NO@Ti–SiC_{sh}; and (d) NO₂@Ti–SiC_{sh} as the selective gas detectors.

The adsorptive capacity of CO, CO₂, NO, and NO₂ on the surface of Ti–SiC_{sh} is approved by the $\Delta E_{\text{ads}}^{\circ}$ amounts as formula:

$$\Delta E_{\text{ads}}^{\circ} = \Delta E_{\text{X} \rightarrow \text{Ti-SiC}_{\text{sh}}}^{\circ} - (\Delta E_{\text{X}}^{\circ} + \Delta E_{\text{Ti-SiC}_{\text{sh}}}^{\circ}); (\text{X} = \text{CO}, \text{CO}_2, \text{NO}, \text{NO}_2).$$

Table 3 has shown that the adsorbing of CO, CO₂, NO, and NO₂ on the surface of Ti–SiC_{sh} must have both “physical” and “chemical” nature. All the measured relative adsorption energies ($\Delta E_{\text{ads}}^{\circ}$) are almost identical, and exhibit the accord of the estimated data by all methods and the accuracy of the calculations. In fact, Ti–SiC_{sh} has higher interaction energy from Van der Waals’ forces with gas molecules including CO, CO₂, NO, and NO₂ that can make them highly stable.

Furthermore, the difference of ΔHR among adsorption of CO, CO₂, NO, and NO₂ on the surface of Ti-doped SiC_{sh} has been unraveled due to non-covalent binding resulted from interatomic interactions between gas molecules and surface (GM@Ti–SiC) and covalent binding resulted from intra-atomic interactions between transition metal of titanium and silicon carbide nanosheet (Ti–SiC_{sh}) (**Table 3**). For the adsorption mechanism, ΔG_{ads} is calculated as follows:

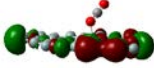
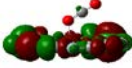
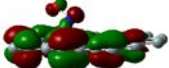
$$\Delta G_{\text{ads}}^{\circ} = \Delta G_{\text{X} \rightarrow \text{Ti-SiC}_{\text{sh}}}^{\circ} - (\Delta G_{\text{X}}^{\circ} + \Delta G_{\text{Ti-SiC}_{\text{sh}}}^{\circ}); (\text{X} = \text{CO}, \text{CO}_2, \text{NO}, \text{NO}_2).$$

On the basis of data in **Table 3**, it is predicted that the adsorption of the gas molecules on the Ti–SiC_{sh} surface might be physical and chemical nature. As shown in **Table 3**, all the computed ΔG_{ads} amounts are close, which exhibits the accord of the evaluated data by all methods and the validity of the computations. However, Ti–SiC_{sh} surface seems possess enough efficiency for adsorption of gas molecules containing CO, CO₂, NO, and NO₂ through charge transfer from nitrogen and oxygen to the titanium element doping of silicon carbide due to intra-atomic and interatomic interactions.

3.5. Analysis of HOMO & LUMO

Based on frontier molecular orbital (FMO) theory, the low unoccupied molecular orbital (LUMO) and the high occupied molecular orbital (HOMO) and the energy between them is the band gap of the adsorption system were computed. In fact, broad band gap diagram indicates that there is less conductivity^[65–67]. The LUMO, HOMO, band energy gap (ΔE) and other quantities distributions of CO, CO₂, NO, and NO₂ on the surfaces of Ti–SiC_{sh} as the gas detector systems denote that the gas adsorption procedure scatters the electrons of the system (**Table 4**).

Table 4. LUMO (eV), HOMO (eV), band energy gap (ΔE /eV) and other quantities (eV) distributions of CO, CO₂, NO, and NO₂ on the surfaces of Ti–SiC_{sh}.

Gas → Ti–SiC	LUMO	HOMO	ΔE	μ	χ	η	ζ	ψ
CO@Ti–SiC	 0.6038	 -0.2710	0.8748	0.1664	-0.1664	0.4374	1.1431	0.0316
CO ₂ @Ti–SiC	 0.8560	 0.0114	0.8674	0.4223	-0.4223	0.4337	1.1528	0.2056
NO@Ti–SiC	 0.6011	 -1.1907	1.7918	-0.2948	0.2948	0.8959	0.5581	0.0485
NO ₂ @Ti–SiC	 0.4933	 -1.4947	1.988	-0.5007	0.5007	0.994	0.5030	0.1261

Band energy gap: $\Delta E = E_{\text{LUMO}} - E_{\text{HOMO}}$; Chemical potential: $\mu = (E_{\text{HOMO}} + E_{\text{LUMO}})/2$; Electronegativity: $\chi = -(E_{\text{HOMO}} + E_{\text{LUMO}})/2$; Hardness: $\eta = (E_{\text{LUMO}} - E_{\text{HOMO}})/2$; Softness: $\zeta = 1/(2\eta)$; electrophilicity index: $\psi = \mu^2/(2\eta)$.

The energy gap between HOMO and LUMO has represented the transporting of molecular electrical characters^[68]. On the other hand, the difference between HOMO and LUMO has exhibited that the effect of the adsorption process on the electronic behavior of CO, CO₂, NO, and NO₂ on the surfaces of Ti–SiC_{sh} nanosheet (**Table 4**). Other quantities (eV) consisting of chemical potential, electronegativity, hardness, softness, and electrophilicity index show an agreeable yield for capturing CO, CO₂, NO, and NO₂ by Ti–SiC_{sh} nanosheet (**Table 4** and **Figure 4**).

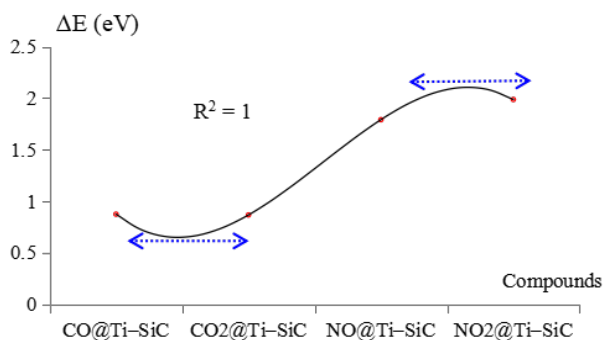


Figure 4. The band energy gap (ΔE) for adsorption of CO, CO₂, NO, and NO₂ on the surfaces of Ti–SiC_{sh} nanosheet and formation of CO@Ti–SiC, CO₂@Ti–SiC, NO@Ti–SiC and NO₂@Ti–SiC complexes with relation coefficient of $R^2 = 1$.

The illustration of donor–acceptor molecules depends on the relative frontier molecular levels. The HOMO-LUMO gap defines the charge transfer in gas molecules adsorbed on the Ti–SiC_{sh} nanosheet through simplified molecular-level diagram. In fact, the amount of transferred charges might be considerably small, as in the case of parallel and perpendicular coordination, which indicate electronic couplings smaller than in co-facial coordination. The results in **Table 4** have indicated the energy level shifts of gas molecule → surface-HOMO and gas molecule → surface-LUMO of nanoclusters as a function of their distance d orbitals from the high symmetry points of each gas molecule on the Ti–SiC_{sh} nanosheet. Therefore, the HOMO level of molecule is being lowered as it loses its electron, whereas the LUMO level of surface is being raised as it gains partial charge (**Figure 4**).

4. Conclusions

In this article, it was indicated that the silicon carbide (SiC) as a sensor can be sensitive to doping with the transition metal when it shows an acceptable response to gas molecules adsorption. The current research wanted to remark the illustration of gas adsorption on Ti–SiC_{sh} nanosheet. Particularly, the structural, energetic, and infrared adsorption properties of linearly “atop” for CO, CO₂, NO, and NO₂ gas molecules adsorbing on Ti–SiC_{sh} nanosheet has been explored by using DFT calculations.

The values of changes of charge density have shown a more important charge transfer for Ti–SiC_{sh} nanosheet which acts as the electron acceptor while gas molecules act as the stronger electron donors through adsorption on the Ti–SiC_{sh} nanosheet surface. It has been assumed that the priority for selecting the surface binding of N-atom of NO, and O-atom of NO₂, CO and CO₂ in adsorption site can be impacted by the existence of close atoms in the Ti–SiC_{sh} surface.

In fact, Ti site in SiC_{sh} nanosheet has higher interaction energy from Van der Waals’ forces with gas molecules including CO, CO₂, NO, and NO₂ that can make them highly stable. Finally, our molecular simulation consequences have exhibited the existence of orbital hybridization between titanium site and gas molecules of CO, CO₂, NO, and NO₂ that also approves the recovery of adsorption susceptibility of graphene sheet. In fact, Ti–SiC_{sh} surface can promise an applicable outlook in the field of CO, CO₂, NO, and NO₂ gas sensor. In the future work, the author aims to evaluate the efficiency of monolayered carbides of main

group elements including Si, Ge, Sn and Pb for gas adsorption through their geometrical and electromagnetic and thermodynamic properties using density functional (DFT) calculations.

Acknowledgments

In successfully completing this paper and its research, the author is grateful to Kastamonu University for their support through the office, library, and scientific websites.

Conflict of interest

The author declares no conflict of interest.

References

1. Rodin AS, Carvalho A, Castro Neto AH. Strain-induced gap modification in black phosphorus. *Physical Review Letters* 2014; 112(17): 176801. doi: 10.1103/PhysRevLett.112.176801
2. Low T, Rodin AS, Carvalho A, et al. Tunable optical properties of multilayer black phosphorus thin films. *Physical Review B* 2014; 90(7): 075434. doi: 10.1103/PhysRevB.90.075434
3. Fei R, Faghaninia A, Soklaski R, et al. Enhanced thermoelectric efficiency via orthogonal electrical and thermal conductances in phosphorene. *Nano Letters* 2014; 14(11): 6393–6399. doi: 10.1021/nl502865s
4. Ramasubramanian A, Muniz AR. *Ab initio* studies of thermodynamic and electronic properties of phosphorene nanoribbons. *Physical Review B* 2014; 90(8): 085424. doi: 10.1103/PhysRevB.90.085424
5. Novoselov KS, Geim AK, Morozov SV, et al. Electric field effect in atomically thin carbon films. *Science* 2004; 306(5696): 666–669. doi: 10.1126/science.1102896
6. Geim AK. Graphene: Status and prospects. *Science* 2009; 324(5934): 1530–1534. doi: 10.1126/science.1158877
7. Neto AHC, Guinea F, Peres NMR, et al. The electronic properties of graphene. *Reviews of Modern Physics* 2009; 81(1): 109. doi: 10.1103/RevModPhys.81.109
8. Mak KF, Lee C, Hone J, et al. Atomically thin MoS₂: A new direct-gap semiconductor. *Physical Review Letters* 2010; 105(13): 136805. doi: 10.1103/PhysRevLett.105.136805
9. Mollaamin F, Monajjemi M. Corrosion inhibiting by some organic heterocyclic inhibitors through langmuir adsorption mechanism on the Al-X (X = Mg/Ga/Si) alloy surface: A study of quantum three-layer method of CAM-DFT/ONIOM. *Journal of Bio- and Tribo-Corrosion* 2023; 9: 33. doi: 10.1007/s40735-023-00751-y
10. Mollaamin F, Monajjemi M. Doping of graphene nanostructure with iron, nickel and zinc as selective detector for the toxic gas removal: A density functional theory study. *C* 2023; 9(1): 20. doi: 10.3390/c9010020
11. Yan Z, Bai Y, Sun L. Adsorption of thiophene and SO_x molecules on Cr-doped and Ti-doped graphene nanosheets: A DFT study. *Materials Research Express* 2019; 6(12): 125067. doi: 10.1088/2053-1591/ab599d
12. Mollaamin F, Monajjemi M. Graphene embedded with transition metals for capturing carbon dioxide: Gas detection study using QM methods. *Clean Technologies* 2023; 5(1): 403–417. doi: 10.3390/cleantechnol5010020
13. Mollaamin F, Monajjemi M. Transition metal (X = Mn, Fe, Co, Ni, Cu, Zn)-doped graphene as gas sensor for CO₂ and NO₂ detection: A molecular modeling framework by DFT perspective. *Journal of Molecular Modeling* 2023; 29(4): 119. doi: 10.1007/s00894-023-05526-3
14. Mollaamin F, Monajjemi M. Tailoring and functionalizing the graphitic-like GaN and GaP nanostructures as selective sensors for NO, NO₂, and NH₃ adsorbing: A DFT study. *Journal of Molecular Modeling* 2023; 29(6): 170. doi: 10.1007/s00894-023-05567-8
15. Mollaamin F, Monajjemi M. Application of DFT and TD-DFT on langmuir adsorption of nitrogen and sulfur heterocycle dopants on an aluminum surface decorated with magnesium and silicon. *Computation* 2023; 11(6): 108. doi: 10.3390/computation11060108
16. Zhang XH, Han JC, Zhou JG, et al. Ferromagnetism in homogeneous (Al, Co)-codoped 4H-silicon carbides. *Journal of Magnetism and Magnetic Materials* 2014; 363: 34–42. doi: 10.1016/j.jmmm.2014.03.062
17. Monajjemi M, Mahdavian L, Mollaamin F. Characterization of nanocrystalline silicon germanium film and nanotube in adsorption gas by Monte Carlo and Langevin dynamic simulation. *Bulletin of the Chemical Society of Ethiopia* 2008; 22(2): 277–286. doi: 10.4314/bcse.v22i2.61299
18. Lin SS. Light-emitting two-dimensional ultrathin silicon carbide. *The Journal of Physical Chemistry C* 2012; 116(6): 3951–3955. doi: 10.1021/jp210536m
19. Hsueh HC, Guo GY, Louie SG. Excitonic effects in the optical properties of a SiC sheet and nanotubes. *Physical Review B* 2011; 84: 085404. doi: 10.1103/PhysRevB.84.085404
20. Eliseeva NS, Kuzubov AA, Ovchinnikov SG, et al. Theoretical study of the magnetic properties of ordered vacancies in 2D hexagonal structures: Graphene, 2D-SiC, and H-BN. *JETP Letters* 95: 555–559. doi: 10.1134/S0021364012110045

21. Mollaamin F, Monajjemi M. electric and magnetic evaluation of aluminum–magnesium nanoalloy decorated with germanium through heterocyclic carbenes adsorption: A density functional theory study. *Russian Journal of Physical Chemistry B* 2023; 17(3): 658–672. doi: 10.1134/S1990793123030223
22. Gaiardo A, Fabbri B, Valt M, et al. Silicon carbide: A gas sensing material for selective detection of SO₂. *Proceedings* 2017; 1(8): 745. doi: 10.3390/proceedings1080745
23. Litvinov A, Etrekova M, Podlepetsky B, et al. MOSFE-capacitor silicon carbide-based hydrogen gas sensors. *Sensors* 2023; 23(7): 3760. doi: 10.3390/s23073760
24. Samotaev N, Litvinov A, Oblov K, et al. Combination of material processing and characterization methods for miniaturization of field-effect gas sensor. *Sensors* 2023; 23(1): 514. doi: 10.3390/s23010514
25. Jin Q, Yuan J, Zhou J. Surface modification of silicon carbide wafers using atmospheric plasma etching: Effects of processing parameters. *Micromachines* 2023; 14(7): 1331. doi: 10.3390/mi14071331
26. Xu S, Yuan J, Zhou J, et al. Study of atmospheric pressure plasma temperature based on silicon carbide etching. *Micromachines* 2023; 14(5): 992. doi: 10.3390/mi14050992
27. Bekaroglu E, Topsakal M, Cahagirov S, Ciraci S. First-principles study of defects and adatoms in silicon carbide honeycomb structures. *Physical Review B* 2010; 81(7): 075433. doi: 10.1103/PhysRevB.81.075433
28. Alaal N, Loganathan V, Medhekar N, Shukla A. First principles many-body calculations of electronic structure and optical properties of SiC nanoribbons. *Journal of Physics D: Applied Physics* 2016; 49(10): 105306. doi: 10.1088/0022-3727/49/10/105306
29. Javan MB. Electronic and magnetic properties of monolayer SiC sheet doped with 3d-transition metals. *Journal of Magnetism and Magnetic Materials* 2016; 401: 656–661. doi: 10.1016/j.jmmm.2015.10.103
30. Wu Y, Zhou L, Du X, Yang Y. Near-field radiative heat transfer between two SiC plates with/without coated metal films. *Journal of Nanoscience and Nanotechnology* 2015; 15(4): 3017–3024. doi: 10.1166/jnn.2015.9687
31. Chabi S, Guler Z, Brearley AJ, et al. The creation of true two-dimensional silicon carbide. *Nanomaterials* 2023; 11(7): 1799. doi: 10.3390/nano11071799
32. Galashev AE. Computer simulation of a silicene anode on a silicon carbide substrate. *Russian Journal of Physical Chemistry B* 2023; 17(1): 113–121. doi: 10.1134/S1990793123010190
33. Shikunov S, Kaledin A, Shikunova I, et al. Novel method for deposition of gas-tight SiC coatings. *Coatings* 2023; 13(2): 354. doi: 10.3390/coatings13020354
34. Makhov MN. Energy content of HMX–Silicon nanopowder mixtures. *Russian Journal of Physical Chemistry B* 2018; 12(1): 115–119. doi: 10.1134/S1990793118010232
35. Yadav A. Monolayer silicon carbide as an efficient adsorbent for volatile organic compounds: An *Ab initio* approach. *Silicon* 2023; 15(3): 1563–1569. doi: 10.1007/s12633-022-02120-9
36. Yadav A. Monolayered carbides of main group elements (Si, Ge, Sn and Pb) for NO₂ gas sensing: Insights from first-principle studies. *Silicon* 2022; 14(18): 12683–12692. doi: 10.1007/s12633-022-01987-y
37. Dindorkar SS, Yadav A. Comparative study on adsorption behaviour of the monolayer graphene, boron nitride and silicon carbide hetero-sheets towards carbon monoxide: Insights from first-principle studies. *Computational and Theoretical Chemistry* 2022; 1211: 113676. doi: 10.1016/j.comptc.2022.113676
38. Dindorkar SS, Yadav A. Monolayered silicon carbide for sensing toxic gases: A comprehensive study based on the first-principle density functional theory. *Silicon* 2022; 14(17): 11771–11779. doi: 10.1007/s12633-022-01899-x
39. Mollaamin F, Monajjemi M. Graphene-based resistant sensor decorated with Mn, Co, Cu for nitric oxide detection: Langmuir adsorption & DFT method. *Sensor Review* 2023; 43(4): 266–279. doi: 10.1108/SR-03-2023-0040
40. Perdew JP, Burke K, Ernzerhof M. Generalized gradient approximation made simple. *Physical Review Letters* 1996; 77(18): 3865–3868. doi: 10.1103/PhysRevLett.77.3865
41. Mollaamin F, Monajjemi M. Tribocorrosion framework of (Iron, Nickel, Zinc)-doped graphene nanosheet: New sights into sulfur dioxide and hydrogen sulfide removal using DFT/TD-DFT methods. *Journal of Bio- and Tribo-Corrosion* 2023; 9(3): 47. doi: 10.1007/s40735-023-00768-3
42. Miyamoto Y, Yu BD. Computational designing of graphitic silicon carbide and its tubular forms. *Applied Physics Letters* 2002; 80(4): 586–588. doi: 10.1063/1.1445474
43. Mollaamin F, Monajjemi M. Hexagonal honeycomb PL-GaN nanosheet as adsorbent surface for gas molecules sensing: A quantum chemical study. *Surface Review and Letters* 2023. doi: 10.1142/S0218625X24500057
44. Monajjemi M, Mollaamin F, Gholami MR, et al. Quantum chemical parameters of some organic corrosion inhibitors, pyridine, 2-Picoline 4-Picoline and 2,4-Lutidine, adsorption at aluminum surface in hydrochloric and nitric acids and comparison between two acidic media. *Main Group Metal Chemistry* 2003; 26(6): 349–361. doi: 10.1515/MGMC.2003.26.6.349
45. Dennington R, Keith TA, Millam J. GaussView Version 6. Available online: <https://gaussian.com/gaussview6/> (accessed on 11 February 2023).
46. Frisch MJ, Trucks GW, Schlegel HB, et al. Gaussian 16, Revision C.01, Gaussian, Inc., Wallingford CT, 2016. Available online: <https://gaussian.com/> (accessed on 24 September 2021).
47. Dzedzej Z, Gzella T. Generalized gradient equivariant multivalued maps, approximation and degree. *Mathematics* 2020; 8(8): 1262. doi: 10.3390/math8081262

48. Bakhshi K, Mollaamin F, Monajjemi M. Exchange and correlation effect of hydrogen chemisorption on nano V(100) surface: A DFT study by generalized gradient approximation (GGA). *Journal of Computational and Theoretical Nanoscience* 2011; 8(4): 763–768. doi: 10.1166/jctn.2011.1750
49. Monajjemi M, Baie MT, Mollaamin F. Interaction between threonine and cadmium cation in $[\text{Cd}(\text{Thr})_n]^{2+}$ ($n = 1-3$) complexes: Density functional calculations. *Russian Chemical Bulletin* 2010; 59(5): 886–889. doi: 10.1007/s11172-010-0181-5
50. Mollaamin F, Monajjemi M, Salemi S, Baei MT. A dielectric effect on normal mode analysis and symmetry of BNNT nanotube. *Fullerenes, Nanotubes and Carbon Nanostructures* 2011; 19(3): 182–196. doi: 10.1080/15363831003782932
51. Khaleghian M, Zahmatkesh M, Mollaamin F, Monajjemi M. Investigation of solvent effects on armchair single-walled carbon nanotubes: A QM/MD study. *Fullerenes, Nanotubes and Carbon Nanostructures* 2011; 19(4): 251–261. doi: 10.1080/15363831003721757
52. Monajjemi M, Khaleghian M, Tadayonpour N, Mollaamin F. The effect of different solvents and temperatures on stability of single-walled carbon nanotube: A QM/MD study. *International Journal of Nanoscience* 2011; 9(5): 517–529. doi: 10.1142/S0219581X10007071
53. Korhonen ST, Calatayud M, Krause AOI. Stability of hydroxylated (111) and (101) surfaces of monoclinic zirconia: A combined study by DFT and infrared spectroscopy. *The Journal of Physical Chemistry C* 2008; 112(16): 6469–6476. doi: 10.1021/jp8008546
54. Crocombette JP, Willaime F. *Ab initio* electronic structure calculations for nuclear materials. *Comprehensive Nuclear Materials* 2012; 1: 223–248. doi: 10.1016/B978-0-08-056033-5.00025-2
55. Svensson M, Humbel S, Froese RDJ, et al. ONIOM: A multilayered integrated MO + MM method for geometry optimizations and single point energy predictions. A test for Diels–alder reactions and $\text{Pt}(\text{P}(t\text{-Bu})_3)_2 + \text{H}_2$ oxidative addition. *The Journal of Physical Chemistry* 1996; 100(50): 19357–19363. doi: 10.1021/jp962071j
56. Lehtola S. A review on non-relativistic fully numerical electronic structure calculations on atoms and diatomic molecules. *International Journal of Quantum Chemistry* 2019; 119(19): e25968. doi: 10.1002/qua.25968
57. Henkelman G, Arnaldsson A, Jónsson H. A fast and robust algorithm for Bader decomposition of charge density. *Computational Materials Science* 2006; 36(3): 354–360. doi: 10.1016/j.commatsci.2005.04.010
58. Zhou YG, Zu XT, Gao F, et al. Electronic and magnetic properties of graphene adsorbed with S atom: A first-principles study. *Journal of Applied Physics* 2009; 105(10): 104311. doi: 10.1063/1.3130401
59. Mao Y, Yuan J, Zhong J. Density functional calculation of transition metal adatom adsorption on graphene. *Journal of Physics: Condensed Matter* 2008; 20(11): 115209. doi: 10.1088/0953-8984/20/11/115209
60. Smith JAS. Nuclear quadrupole resonance spectroscopy. General principles. *Journal of Chemical Education* 1971; 48(1): 39. doi: 10.1021/ed048p39
61. Trontelj Z, Pirnat J, Jazbinšek V, et al. Nuclear quadrupole resonance (NQR)—A useful spectroscopic tool in pharmacy for the study of polymorphism. *Crystals* 2020; 10(6): 450. doi: 10.3390/cryst10060450
62. Larina LI. Nuclear quadrupole resonance spectroscopy: Tautomerism and structure of functional azoles. *Crystals* 2019; 9(7): 366. doi: 10.3390/cryst9070366
63. Young HD, Freedman RA, Lewis FA. *Sears and Zemansky's University Physics with Modern Physics*, 13th ed. Addison-Wesley; 2011. p. 754.
64. Mollaamin F, Monajjemi M. Molecular modelling framework of metal-organic clusters for conserving surfaces: Langmuir sorption through the TD-DFT/ONIOM approach. *Molecular Simulation* 2023; 49(4): 365–376. doi: 10.1080/08927022.2022.2159996
65. Mollaamin F, Shahriari S, Monajjemi M, Khalaj Z. Nanocluster of aluminum lattice via organic inhibitors coating: A study of freundlich adsorption. *Journal of Cluster Science* 2023; 34(3): 1547–1562. doi: 10.1007/s10876-022-02335-1
66. Monajjemi M, Baheri H, Mollaamin F. A percolation model for carbon nanotube-polymer composites using the Mandelbrot-given. *Journal of Structural Chemistry* 2011; 52(1): 54–59. doi: 10.1134/S0022476611010070
67. Mollaamin F, Monajjemi M. In silico-DFT investigation of nanocluster alloys of Al-(Mg, Ge, Sn) coated by nitrogen heterocyclic carbenes as corrosion inhibitors. *Journal of Cluster Science* 2023. doi: 10.1007/s10876-023-02436-5
68. Mollaamin F, Ilkhani A, Sakhaei N, et al. Thermodynamic and solvent effect on dynamic structures of nano bilayer-cell membrane: Hydrogen bonding study. *Journal of Computational and Theoretical Nanoscience* 2015; 12(10): 3148–3154. doi: 10.1166/jctn.2015.4092